**Atmospheric
Chemistry
and Physics**

Assimilation of ground versus lidar observations for PM$_{10}$ forecasting

Y. Wang[1,2], **K. N. Sartelet**[1], **M. Bocquet**[1,3], **and P. Chazette**[2]

[1]CEREA, joint laboratory Ecole des Ponts ParisTech - EDF R&D, Université Paris-Est, 77455 Champs sur Marne, France
[2]LSCE, joint laboratory CEA-CNRS, UMR8212, 91191 Gif-sur-Yvette, France
[3]INRIA, Paris-Rocquencourt Research Center, Le Chesnay, France

Correspondence to: Y. Wang (wangy@cerea.enpc.fr)

Abstract. This article investigates the potential impact of future ground-based lidar networks on analysis and short-term forecasts of particulate matter with a diameter smaller than 10 μm (PM$_{10}$). To do so, an Observing System Simulation Experiment (OSSE) is built for PM$_{10}$ data assimilation (DA) using optimal interpolation (OI) over Europe for one month from 15 July to 15 August 2001. First, using a lidar network with 12 stations and representing the "true" atmosphere by a simulation called "nature run", we estimate the efficiency of assimilating the lidar network measurements in improving PM$_{10}$ concentration for analysis and forecast. It is compared to the efficiency of assimilating concentration measurements from the AirBase ground network, which includes about 500 stations in western Europe. It is found that assimilating the lidar observations decreases by about 54 % the root mean square error (RMSE) of PM$_{10}$ concentrations after 12 h of assimilation and during the first forecast day, against 59 % for the assimilation of AirBase measurements. However, the assimilation of lidar observations leads to similar scores as AirBase's during the second forecast day. The RMSE of the second forecast day is improved on average over the summer month by 57 % by the lidar DA, against 56 % by the AirBase DA. Moreover, the spatial and temporal influence of the assimilation of lidar observations is larger and longer. The results show a potentially powerful impact of the future lidar networks. Secondly, since a lidar is a costly instrument, a sensitivity study on the number and location of required lidars is performed to help define an optimal lidar network for PM$_{10}$ forecasts. With 12 lidar stations, an efficient network in improving PM$_{10}$ forecast over Europe is obtained by regularly spacing the lidars. Data assimilation with a lidar network of 26 or 76 stations is compared to DA with the previously-used lidar network. During the first forecast day, the assimilation of 76 lidar stations' measurements leads to a better score (the RMSE decreased by about 65 %) than Air-Base's (the RMSE decreased by about 59 %).

1 Introduction

Aerosols have an impact on regional and global climates (Ramanathan et al., 2001; Léon et al., 2002; Sheridan et al., 2002; Intergovernment Panel on Climate Control , IPCC 2007) as well as on ecological equilibrium (Barker and Tingey, 1992) and human health by penetrating the respiratory system and leading to respiratory and cardiovascular diseases (Lauwerys et al., 2007; Dockery and Pope, 1996). Aerosols influence the photo-dissociation of gaseous molecules (Randriamiarisoa et al., 2004) and can thus have a significant impact on photochemical smog (Dickerson et al., 1997). Thus the accurate prediction of aerosol concentration levels has signification human and economic cost implications.

Various chemistry transport models are used to simulate or predict aerosol concentrations over Europe, e.g. EMEP (European Monitoring and Evaluation Programme) (Simpson et al., 2003), LOTOS (Long Term Ozone Simulation) – EUROS (European Operational Smog) (Schaap et al., 2004), CHIMERE (Hodzic et al., 2006), DEHM (Danish Eulerean Hemispheric Model) (Brandt et al., 2007) and POLYPHEMUS (Sartelet et al., 2007). However, uncertainties in modelling atmospheric components, in particular aerosols are

high (Roustan et al., 2010), which leads to significant differences between model simulations and observations (Sartelet et al., 2007). Data assimilation (DA hereafter) can reduce the uncertainties in input data such as the initial conditions or the boundary conditions by coupling models to observations (Bouttier and Courtier, 2001). In meteorology, DA has been traditionally applied to improve forecasts (Kalnay et al., 2003; Lahoz et al., 2010). In air quality, Zhang et al. (2012) review chemical DA techniques developed to improve regional real-time air quality forecasting model performance for ozone, PM_{10}, and dust. However, applications of DA to PM_{10} forecasts are still sparse. They include Tombette et al. (2009) and Denby et al. (2008) over Europe and Pagowski et al. (2010) over the United States of America. They demonstrated the feasibility and the usefulness of DA for aerosol forecasts.

As in Tombette et al. (2009), in situ surface measurements are often assimilated, e.g. AirBase, BDQA (Base de Données de la Qualité de l'Air) or EMEP. However, they do not provide information on vertical profiles. Niu et al. (2008) used both satellite retrieval data and surface observations to assimilate dust for sand and dust storm (SDS) forecasts. They found that information on the vertical profiles of the SDS was needed for the SDS forecasts. Although satellite passive remote sensing can provide vertical observations, it is very expensive and data are often limited to low horizontal (e.g. $10 \times 10 \, km^2$ for the Moderate Resolution Imaging Spectroradiometers (MODIS) (Kaufman et al., 2002)) and temporal resolutions (e.g., approximately twice a day for polar orbiting satellites). Passive instruments can only retrieve column-integrated aerosol concentration (Kaufman et al., 2002). Spaceborne lidar promises to improve the vertical resolution of aerosol measurements at the global scale (Winker et al., 2003; Berthier et al., 2006; Chazette et al., 2010). Nevertheless, the spaceborne lidar measurements are only performed along the satellite ground track.

Thanks to the new generation of portable lidar systems developed in the past five years, accurate vertical profiles of aerosols can now be measured (Raut and Chazette, 2007; Chazette et al., 2007). Such instruments document the mid and lower troposphere by means of aerosol optical properties. Lidar measurements were used in several campaigns, such as ESQUIF (Étude et Simulation de la Qualité de l'air en Île-de-France) (Chazette et al., 2005), MEGAPOLI (Megacities: Emissions, urban, regional and Global Atmospheric POLlution and climate effects, and Integrated tools for assessment and mitigation) summer experiment in July 2009 (Royer et al., 2011) and during the eruption of the Icelandic volcano Eyjafjallajökull on 14 April 2010 (Chazette et al., 2012). Raut et Chazette (2009) established a reliable relation between the mass concentration and the optical properties of PM_{10}. Because the surface-to-mass ratio for fine particles ($PM_{2.5}$, particulate matter with a diameter smaller than 2.5 μm) is high, they largely contribute to the measured lidar signal. However, the contribution of coarse particles may not

be negligible as shown by Randriamiarisoa et al. (2006) who estimated it to be about 19 %. The relative contribution of $PM_{2.5}$ may increase with altitude (Chazette et al., 2005), but it is difficult to quantify. Thereby, the PM_{10} concentrations above urban areas can be retrieved from a ground-based lidar system with an uncertainty of about 25 %.

Because a lidar network with continuous measurements does not yet exist, lidar observations have not yet been used for DA. This work aims to investigate the usefulness of future ground-based lidar network on analyses and short-term forecasts of PM_{10} and to help future lidar network projects to design lidar networks, e.g. number and locations of lidar stations. Building and maintaining observing systems with new instruments is very costly, especially for ground-based lidars. Therefore, an Observing System Simulation Experiment (OSSE) can be used to effectively test proposed observing strategies before a field experiment takes place, and it can provide valuable information for the design of field experiments (Masutani et al., 2010).

An OSSE is constituted by a nature run, simulated observations, and DA experiments. The nature run is usually a simulation from a high-resolution state-of-the-art model forecast, and is used to create observations and validate DA experiments (Chen et al., 2011). Many applications use OSSEs, such as for investigating the accuracy of diagnostic heat and moisture budgets (Kuo et al., 1984), studying carbon dioxide measurements from the Orbiting Carbon Observatory using a four-dimensional variational assimilation (Chevallier et al., 2007; Baker et al., 2010), demonstrating the data impact of Doppler wind lidar (Masutani et al., 2010; Tan et al., 2007), defining quantitative trace carbon monoxide measurement requirements for satellite missions (Edwards et al., 2009), comparing the relative capabilities of two geostationary thermal infrared instruments to measure ozone and carbon monoxide (Claeyman et al., 2011), evaluating the contribution of column aerosol optical depth observations from a future imager on a geostationary satellite (Timmermans et al., 2009), and studying the impact of observational strategies in field experiments on weather analysis and short-term forecasts (Chen et al., 2011).

This paper is organised as follows. Section 2 provides a description of the DA methodology used in this study. Section 3 describes the experiment setup, i.e. the chemistry transport model used and real observations. An OSSE is built in Sect. 4. Results of the OSSE are shown in Sects. 5 and 6. Sensitivity studies with respect to the number and locations of lidar stations are conducted in Sect. 7. The findings are summarised and discussed in Sect. 8.

2   Choice of DA method

Data assimilation couples model with simulated observations in an OSSE. Different DA algorithms may be used, e.g. OI, reduced-rank square root Kalman filter, ensemble Kalman

filter (EnKF) and four-dimensional variational assimilation (4D-Var). Wu et al. (2008) have illustrated their limitations and potentials. They found that in the air quality context the OI provides overall strong performances and it is easy to implement. In terms of performance, the reduced-rank square root Kalman filter is quite similar to the EnKF. Denby et al. (2008) compared two different DA techniques, the OI and EnKF, for assimilating PM_{10} concentration at the European scale. They showed OI can be more effective than the EnKF. Although aerosol assimilation could be performed with 4D-Var (Benedetti and Fisher, 2007), it may be limited to the use of a simplified aerosol model, as it is quite expensive for computation.

In this paper, we use the OI as it is the simpler method for PM_{10} DA and it performs well (Denby et al., 2008; Wu et al., 2008). Furthermore, the OI method can be used in operational mode for real-time forecasts, as the computational cost of OI is low. It was used by Tombette et al. (2009) and Pagowski et al. (2010) for DA of conventional aerosol ground observations. In the OI method, DA is performed at the frequency of measurements to produce analysed concentrations, which are closer to reality (measurements) than forecasts and which are used as initial conditions for the next model iteration. The equation to compute the analysed concentrations from the model concentrations is given by:

$$\mathbf{x}_a = \mathbf{x}_b + \mathbf{B}\mathbf{H}^T \left(\mathbf{H}\mathbf{B}\mathbf{H}^T + \mathbf{R} \right)^{-1} (y - H[\mathbf{x}_b]), \qquad (1)$$

where $\mathbf{x}_a$ is the analysed concentrations, $\mathbf{x}_b$ is the model concentrations, y is the observation vector, H is an operator that maps $\mathbf{x}_b$ to the observational data, $\mathbf{H}$ is the tangent linear operator of H (in the following, the observation operator is linear), $\mathbf{B}$ and $\mathbf{R}$ are respectively the background and observation error covariance matrices. They require the specification of the background and observation error covariance matrices (see Sects. 4.2, 4.4 and 5). The background error covariance matrix determines how the corrections of the concentrations should be distributed over the domain during DA. The observation error covariance matrix specifies instrumental and representativeness errors. As in Tombette et al. (2009), after DA of PM_{10} concentrations, the analysed PM_{10} concentrations are redistributed over the model variables following the initial chemical and size distributions.

3 Experimental setup

3.1 Model

For our study, the chemistry transport model POLAIR3D (Sartelet et al., 2007) of the air-quality platform POLYPHE-MUS, available at http://cerea.enpc.fr/polyphemus/ and described in Mallet et al. (2007) is used. Aerosols are modelled using the SIze-REsolved Aerosol Model (SIREAM-SuperSorgam), which is described in Debry et al. (2007)

and Kim et al. (2011). SIREAM-SuperSorgam includes 20 aerosol species: 3 primary species (mineral dust, black carbon and primary organic species), 5 inorganic species (ammonium, sulphate, nitrate, chloride and sodium) and 12 organic species. It models coagulation and condensation. Five bins logarithmically distributed over the size range 0.01 μm–10 μm are used. The gas chemistry is solved with the chemical mechanism CB05 (Carbon Bond version 5) (Yarwood et al., 2005). POLAIR3D/SIREAM has been used for several applications. For example, it was compared to measurements for gas and aerosols over Europe by Sartelet et al. (2007) and Kim et al. (2010), and it was compared to lidar measurements over Greater Paris by Royer et al. (2011).

3.2 Input data

The modelling domain covers western and part of eastern Europe ([10.5° W, 23° E] × [35° N, 58° N]) with a horizontal resolution of 0.5° × 0.5°. Nine vertical levels are considered from the ground to 12 000 m. The heights of the cell interfaces are 0, 40, 120, 300, 800, 1500, 2400, 3500, 6000 and 12 000 m. The simulations are carried out for one month from 15 July to 15 August 2001, with a time step of 600 s. Meteorological inputs are obtained from reanalysis provided by the European Centre for Medium-Range Weather Forecasts (ECMWF). Anthropogenic emissions of gases and aerosols are generated with the EMEP inventory for 2001. For gaseous boundary conditions, daily means are extracted from outputs of the global chemistry-transport model MOZART2 (Model for OZone And Related chemical Tracers version 2) (Horowitz et al., 2003). For aerosol boundary conditions, daily means are based on outputs of the Goddard Chemistry Aerosol Radiation and Transport model (GOCART) for the year 2001 for sulphate, dust, black carbon and organic carbon (Chin et al., 2000; Sartelet et al., 2007).

3.3 Observational data

In this paper, as in Sartelet et al. (2007) and Tombette et al. (2009), we use the locations of stations of two ground databases for the comparisons to ground data measurements:

- the EMEP database, available on the EMEP Chemical Co-ordinating Centre (EMEP/CCC) web site at http://www.emep.int/;

- the AirBase database, available on the European Environment Agency (EEA) web site at http://air-climate.eionet.europa.eu/databases/airbase/. Note that the traffic and industrial stations are not used, because the simulation horizontal scale (0.5° × 0.5°) can not be representative of these station types.

In 2001, PM_{10} concentrations are provided on a daily basis at EMEP stations, against an hourly basis at most AirBase stations. Moreover, data are provided at only 27 EMEP stations, against 509 AirBase stations. Therefore, the EMEP network

Table 1. Statistics (see Appendix A) of the simulation results for the AirBase and EMEP networks from 15 July to 14 August. Ammon. stands for ammonium. Obs. stands for observation. Sim. stands for simulation. Corr. stands for correlation.

| Species	Database	Stations	Obs. mean $\mu g\, m^{-3}$	Sim. mean $\mu g\, m^{-3}$	RMSE $\mu g\, m^{-3}$	Corr. %	MFB %	MFE %
PM_{10}	AirBase	419	22.5	12.7	17.3	35	−47	69
	EMEP	27	18.8	12.3	9.6	67	−39	48
$PM_{2.5}$	AirBase	3	11.2	13.1	8.7	45	7	44
	EMEP	18	13.2	11.5	7.2	64	−16	45
Sulphate	AirBase	11	2.2	3.0	1.7	59	41	60
	EMEP	51	2.9	2.6	1.7	61	−3	45
Nitrate	AirBase	8	2.8	5.1	4.0	51	23	72
	EMEP	13	1.7	2.2	1.9	20	−16	78
Ammon.	AirBase	8	1.7	2.5	1.3	62	28	43
	EMEP	8	1.6	1.8	1.1	39	6	47
Sodium	EMEP	1	1.4	2.4	1.6	82	44	52
Chloride	AirBase	7	0.6	2.2	1.9	70	1	1
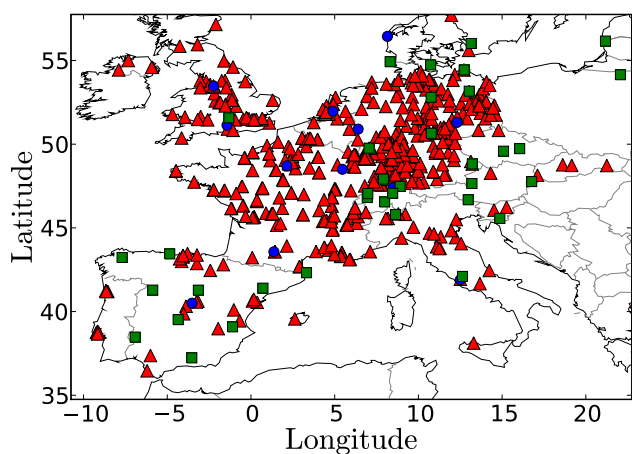
Fig. 1. The green squares show the locations of EMEP stations, the red triangles show the locations of AirBase stations, and the blue discs show the locations of the lidar network.

Fig. 2. Mean concentrations of PM_{10} over Europe (in $\mu g\, m^{-3}$). It ranges from $6\,\mu g\, m^{-3}$ (dark blue) to $34\,\mu g\, m^{-3}$ (dark red).

is only used for the performance assessment of the nature run, whereas the AirBase network is used for both the performance assessment of the nature run and assimilations in the OSSE. Figure 1 shows the location of the EMEP and Air-Base stations used in this study.

In this work, a network of 12 fictitious ground-based lidar stations covering western Europe is defined, as shown in Fig. 1, based on the lidar locations of existing observation stations, e.g. a subset of stations from the European Aerosol Research Lidar Network (http://www.earlinet.org/). A relation between PM_{10} mass concentration and optical properties of aerosols is assumed to exist, although it has so far only been determined for pollution aerosols over Greater Paris (Raut and Chazette, 2009) and it needs to be generalised to other measurement sites.
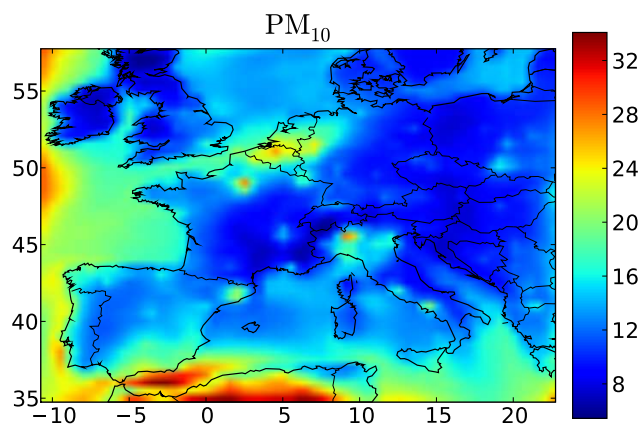
4 Observing system simulation experiment

4.1 Nature run

Observation impact experiments for not-yet-existing observing systems require an atmospheric state, from which the hypothetical observations can be generated. Since the true atmosphere is inherently unknown, a synthetic atmosphere state, in the remainder denoted "truth", needs to be defined. In an OSSE, the "true" state is used to create the observational data from existing and future instruments. In this paper, the "truth" is obtained from a simulation, called nature run, performed between 00:00 UTC 15 July to 00:00 UTC 15 August 2001 using the model (Kim et al., 2010, 2011) and the input data described in the previous section. Here, we first evaluate the results of this simulation with the AirBase and EMEP networks.

For an OSSE study, the accuracy of the nature run compared with real observations is important, and the nature run
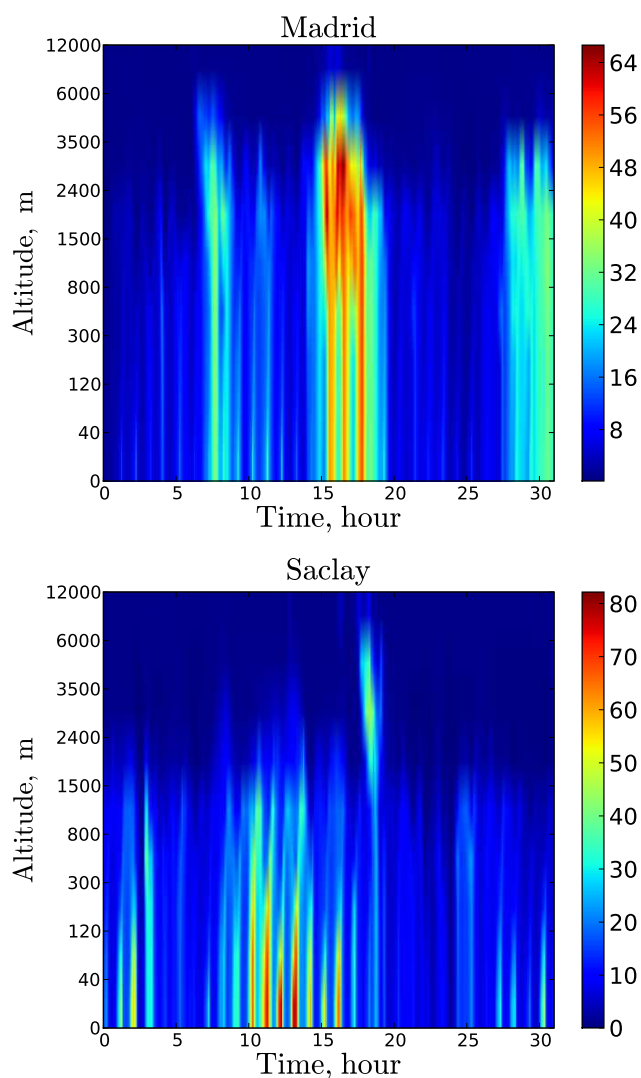
Madrid

Saclay

Fig. 3. The "true" state of PM$_{10}$ from 01:00 UTC 15 July to 00:00 UTC 15 August 2001 at the lidar stations Madrid (upper panel) and Saclay (lower panel). Dark and red colours correspond to high and low PM$_{10}$ concentrations (µg m^{-3}), respectively.

should produce typical features of the phenomena of interest. According to Boylan and Russel (2006), if both the Mean Fractional Bias (MFB) and the Mean Fractional Error (MFE) are in the range [−30 %, 30 %] and [0, 50 %] respectively, then the model performance goal is met; if both the MFB and MFE are in the range [−60 %, 60 %] and [0, 75 %] respectively, the model performance criterion is met. As shown in Table 1, for PM$_{10}$, the model performance criterion is met for the two networks, whereas for PM$_{2.5}$ the model performance goal is met for both networks, suggesting that this simulation compares well to observations. Furthermore, as shown in Fig. 2, the spatial distribution of PM$_{10}$ concentration corresponds to previously published results (Sartelet et al., 2007). This "true" simulation is subsequently used for

the creation of observations from the observing system under investigation and will also be used to evaluate the results of DA experiments, for example the calculation of the Root Mean Square Error (RMSE) and correlation over land grid points from the ground level to the sixth level (1950 m above the ground) against the nature run.

4.2 Simulated observations and error modelling

The "true" state of the atmosphere (the nature run) is used to calculate the concentrations at both stations of the AirBase network and of the future ground-based lidar network. For example for the lidar network, Fig. 3 shows the "true" state of PM$_{10}$ at two arbitrary chosen lidar stations: Madrid (Perez et al., 2004) and Saclay (Raut et Chazette, 2009). We find that the high PM$_{10}$ concentrations in Madrid are mostly made of Sahara dust. Because the AirBase network covers well western Europe and provides in situ surface measurements (which have been used for the performance assessment of the nature run in section 4.1) and because AirBase measurements have been used for DA of PM$_{10}$ (Denby et al., 2008; Tombette et al., 2009), we took AirBase as an assimilation reference network in order to quantitatively show the potential impact of future ground-based lidar networks on analysis and short-term forecasts of PM$_{10}$. However, real observations at AirBase stations are not used for the assimilation, but the "truth" is used to calculate the "true" states (e.g., concentrations), in order to be consistent with the lidar data.

The "true" state at each station is perturbed depending on estimated observation errors. For the network AirBase, the observation errors mainly correspond to the representativeness errors, and they are estimated to be about 35%. For the ground-based lidar network, the observation errors include the representativeness errors (about 35%) and the instrumental errors, which are estimated to be about 25% for PM$_{10}$ concentrations obtained from lidar observations (Raut et Chazette, 2009). These instrumental errors are linked to errors in estimating the extinction coefficients using the inversion of the lidar signal (Klett et al., 1981) and extinction coefficient cross sections. The covariance between the representativeness and instrumental errors is set to zero since they are independent. Finally, the observation errors of the concentrations obtained from the lidar network are estimated to be about 43 % (the square root of the sum of the representativeness error variance and the instrumental error variance, $\sqrt{35\%^2 + 25\%^2}$). Note that when comparing the nature run to the real data, the errors include both the representativeness errors and the model errors. They are therefore different from the observation errors used to perturb the simulated observations.

After defining the observation errors, the observations obtained from the "true" state are perturbed. For each station, let **x** be a vector, whose component x_i is a hourly mean concentration and i depends on vertical level and time. The perturbation is implemented as follows:
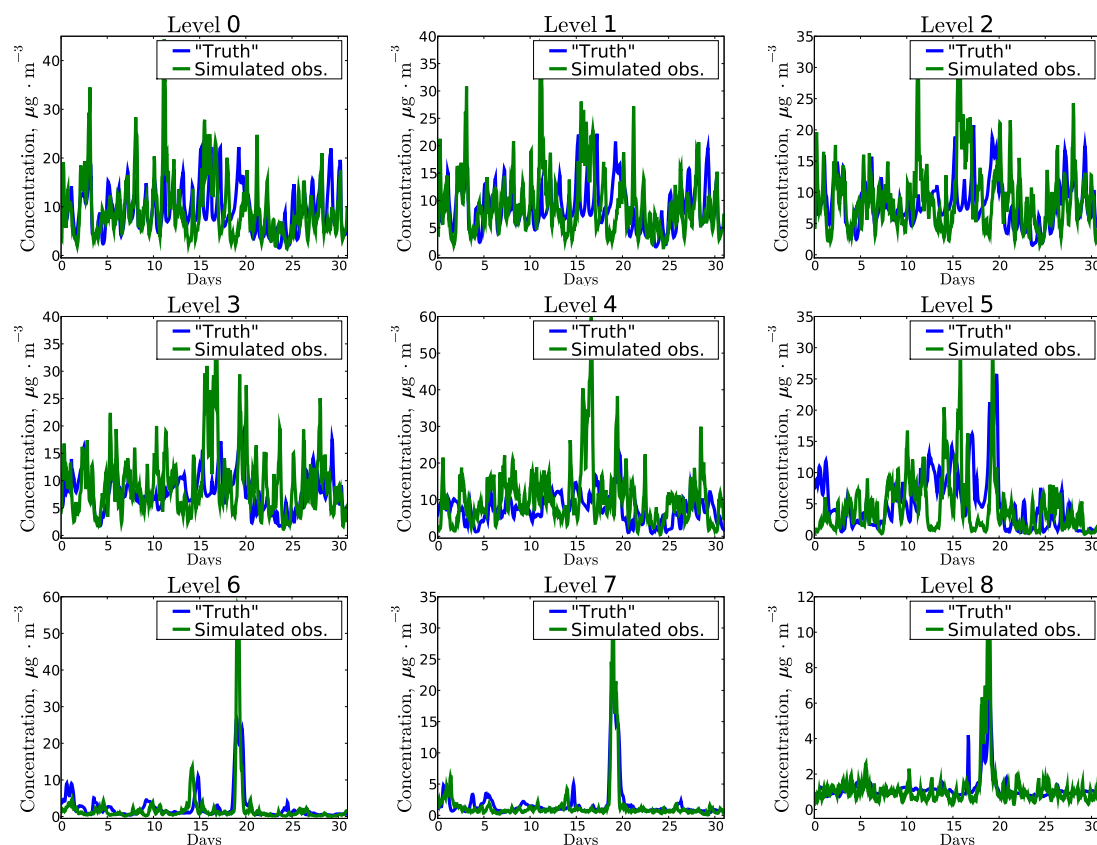
Fig. 4. Perturbation at a random AirBase station from 15 July to 15 August 2001 at from the first vertical level in the model (top left) to the last vertical level in the model (bottom right). The blue lines show the "true" PM_{10} concentrations ($\mu g\,m^{-3}$). The green lines show the simulated PM_{10} concentrations ($\mu g\,m^{-3}$).

– Define the observational error covariance matrix Σ by the Balgovind approach (Balgovind et al., 1983). The error covariance between two points is

$$f(d_v, d_t) = e\left(1 + \frac{d_v}{L_v}\right)\exp\left(-\frac{d_v}{L_v}\right) \times \left(1 + \frac{d_t}{L_t}\right)\exp\left(-\frac{d_t}{L_t}\right), (2)$$

where e is the observational error variance, d_v is the vertical distance between the 2 points, d_t is the temporal difference between the 2 points, $L_v = 200\,m$ and $L_t = 2\,h$ are the vertical and temporal correlation lengths. Each component of the covariance matrix Σ may be written as $\Sigma_{ij} = f\left(d_v(x_i, x_j), d_t(x_i, x_j)\right)$. Each component of the covariance matrix depends smoothly on the altitude of the points and time.

– Use the Cholesky decomposition:

$$\Sigma = \mathbf{C}\mathbf{C}^T, \tag{3}$$

where $\mathbf{C}$ is a lower triangular matrix with strictly positive diagonal entries.

The perturbation of $\mathbf{x}$ is then

$$\mathbf{x}' = \mathbf{x} + \mathbf{C}\gamma, \tag{4}$$

where γ is a random vector whose components are a standard normal distribution (of mean 0 and variance 1). Figure 4 shows an example of perturbations at an arbitrarily chosen station. We can see that the perturbations depend continuously on the vertical level and the time thanks to matrix $\mathbf{C}$. The perturbed observations are subsequently used for the assimilation of the ground-based lidar network and AirBase data.

4.3   Control run

The control run is a simulation that is meant to represent the best modellers' simulation of the atmosphere. If the same model is used for both the nature run and the control run, this is called an identical twin OSSE; if the nature run model is a different version of the control run model, the OSSEs are called fraternal twin OSSEs (Liu et al., 2007; Masutani et al., 2010). We follow a "perfect model" OSSE setup, in which the model used to generate the "true" observations is the same as the one used in the control run and DA. The identical twin OSSEs are easy to set up. However, input data, such as meteorological fields, emissions (Edwards et al., 2009) or initial conditions (Liu et al., 2007) have to be perturbed. In
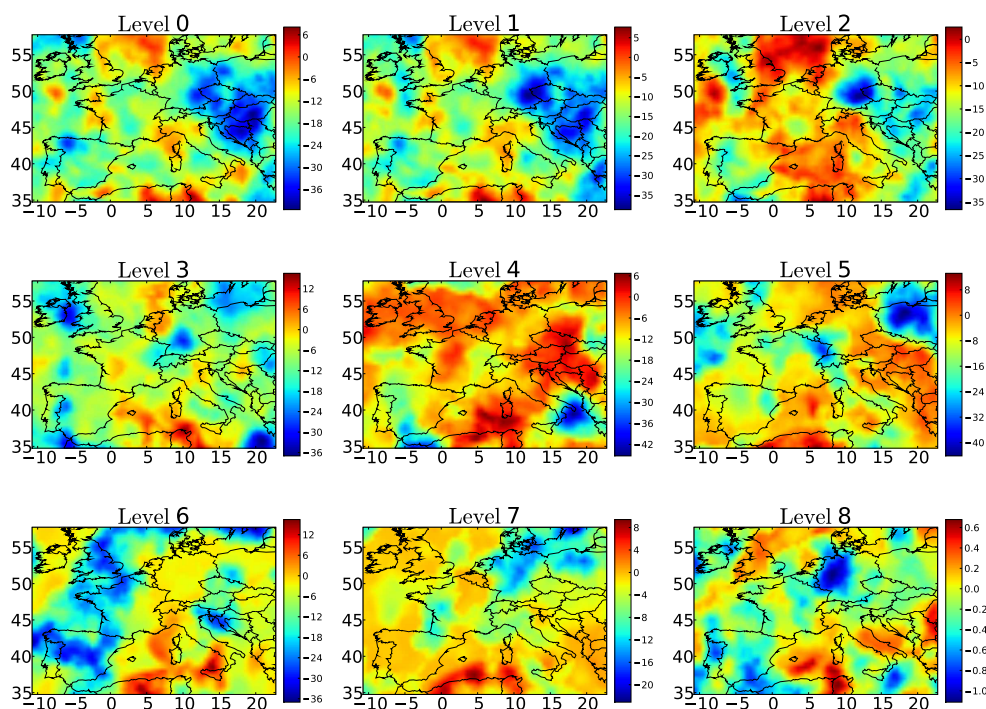
Fig. 5. Differences between "true" and perturbed PM$_{10}$ concentration at 00:00 UTC 15 July 2001, which is the initial time of the first five-day experiment, from the first vertical level in the model (top left) to the last vertical level in the model (bottom right). Differences (µg m^{-3}) vary from negative values in dark blue colour to positive values in dark red colour.

order to be able to interpret more easily the results, we choose to perturb only initial conditions. This allows us to avoid the complications of defining model errors, and the only source of forecast errors comes from the initial conditions. With the identical twin scenario, the numerical model becomes perfect (i.e., no model error); this is counter to what happens in reality (i.e., models are never perfect) and the identical twin OSSEs usually overestimate the impact of observations on model forecasts (Chen et al., 2011).

Although the impact of PM$_{10}$ DA may be over-optimistic, it will be so for both ground observations and lidar observations (the assimilation of both ground and lidar observations lead to corrections at high vertical levels, as discussed in Sect. 5). As in Sect. 4.2, we use the Balvogind approach (Balgovind et al., 1983), the Cholesky decomposition and the normal distribution to perturb all model concentrations (gaseous and aerosols). In air quality models, the impact of initial conditions on PM$_{10}$ concentrations lasts for a few hours to a few days at most. For this impact to last as long as possible, both gaseous and aerosol concentrations are perturbed. As shown in Fig. 5, the differences between "true" and perturbed PM$_{10}$ concentrations in certain parts of Europe are higher than in other parts of Europe. This is due to the normal distribution, which can produce very high or low concentrations in one grid cell. Although the perturbed initial conditions are not necessarily consistent with the true state of atmosphere, they are suitable for our experiments with DA.

4.4 Parameters of the DA runs

The experiments consist of two steps: the DA analysis part and the forecast. During the assimilation period, say between $[t_0, t_N]$, at each time step, the observations are assimilated. During the subsequent forecast period, say between $[t_{N+1}, t_T]$, the aerosol concentrations are obtained from the model simulations initialised from the analysed model state at t_N.

Since only the initial conditions are perturbed in our experiments (see Sect. 4.3), the difference between two forecasts initialised with different initial conditions only lasts for a few days. For the choice of t_N, Fig. 6 compares the RMSE between the true observations and the forecast concentrations from 18 July at 01:00 UTC to 20 July at 00:00 UTC, obtained for different assimilation periods varying from 6 h to 3 days and always ending at 00:00 UTC 18 July. The longer the assimilation period is, the lower the RMSE is. An assimilation period of 12 h seems a good compromise between a low RMSE and a short assimilation time.

Two different types of DA runs are performed in our OSSE, depending on whether ground or vertical observations are assimilated. The simulations use the same setup as the one of the control run. We use the perturbed PM$_{10}$ observations that are produced by the nature run (see Sect. 4.2). The first DA run uses only simulated data at AirBase stations. It is performed from the first level (20 m above the ground) to the sixth level (1950 m above the ground) of the
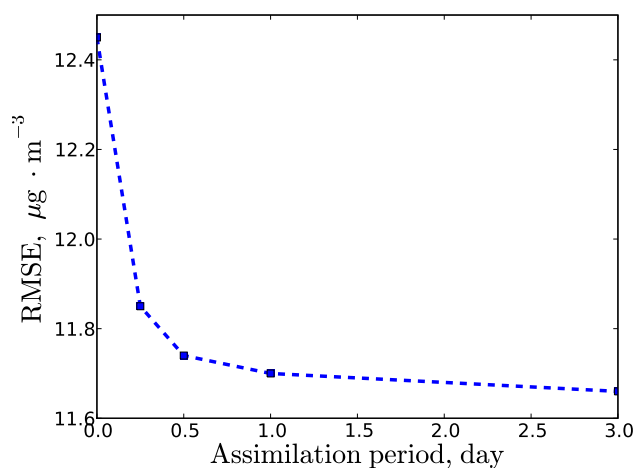
Fig. 6. RMSE (in $\mu g\, m^{-3}$) between the real AirBase observations and forecast concentrations from 18 July to 20 July against assimilation period (in days).

model. The second DA run uses only the ground-based lidar network simulated data. It is performed from the third level (210 m above the ground) to the sixth level (1950 m above the ground), because the lidar measurements are not available from the ground to about 200 m above the ground (Raut et Chazette, 2009; Royer et al., 2011).

In this paper, DA experiments are carried out for 27 five-day experiments between 15 July 2001 and 15 August 2001. The first experiment is from 15 to 19 July 2001, the second one is from 16 to 20 July 2001, and so on until 15 August 2001. For each experiment, the observation data are assimilated from 01:00 UTC to 12:00 UTC every hour, thereafter the model runs and produces a forecast for the next four and half days.

In the OI method, the background and observation error covariance matrices need to be set. The observation error covariance matrix depends on the observational error variance, which varies with vertical levels. For ground measurements, we set the error variance to be $20\,\mu g^2\, m^{-6}$, the square of 35 % (see section 4.2) of PM_{10} concentration averaged over AirBase stations. For lidar measurement, we set the error variance to be the square of 43 % ($\sqrt{35\%^2 + 25\%^2}$, see section 4.2) of PM_{10} concentration averaged over lidar stations for each level from the third level to the sixth level, which is respectively 28, 24, 16 and $5\,\mu g^2\, m^{-6}$.

In the Balgovind parametrisation of the background error covariance matrix (Wu et al., 2008; Tombette et al., 2009), the variance v is set to $60\,\mu g^2\, m^{-6}$, which is obtained from the difference between the nature run and the control run. The correct specification of the background error correlations is crucial to the quality of the analysis, because they determine to what extent the fields will be corrected to match the observations. The horizontal correlation length and the vertical correlation length are two parameters of the Balgovind approach. While the definition of background error correlations is straightforward, since they correspond to the difference between the background state and the true state, the true atmospheric state is never exactly known. The next section details the choice of the horizontal and vertical correlation length.

5   Choice of the horizontal and vertical correlation lengths

The National Meteorological Center (NMC) method (Parrish and Derber, 1992) is used for the choice of the horizontal correlation length L_h and the vertical correlation length L_v. The background error is estimated by the differences of PM_{10} concentrations between two simulations. The two simulations start with the same initial conditions and last 24 hours. A 24 hours forecast is performed in the first simulation, while AirBase data of PM_{10} concentrations are assimilated hourly in the second simulation. In the analysis, the background error covariance matrix is assumed to be a diagonal matrix to avoid adding special error correlations (e.g. the Balgovind approach with a given horizontal and vertical correlation length) in the NMC method. In order to eliminate potential bias due to the diurnal cycle, 24 h forecasts are issued at 00:00 UTC and 12:00 UTC. This estimation of the background error is performed for 27 consecutive days from 15 July 2001 at 00:00 UTC and 12:00 UTC.

To estimate the horizontal correlation length, at each model level, we calculate the covariance value for each site pair. We then obtain a cloud of covariance values. The covariance clouds are averaged within continuous tolerance regions. The length of the tolerance region is set to 4 grid units, so that there are enough site pairs for each tolerance region. Thus, L_h is estimated at all model levels by a least-square fitting of Balgovind functions to the curves of the regionalized covariances (the covariance clouds averaged within tolerance regions). Figure 7 shows the horizontal correlation length L_h of the background error covariance matrix at 00:00 UTC and 12:00 UTC. The variation of the horizontal correlation length is comparable to that of meteorology (Daley , 1991). The horizontal correlation length is relatively constant in the boundary layer, and it is about 4 grid units (200 km). Above the boundary layer, the horizontal correlation length decreases. This is a consequence of the prescribed aerosol boundary conditions and the numerical algorithm. Because the background error is estimated by the differences between a simulation with 24 h forecast and a simulation with assimilating ground measurements in the NMC method (the error sources are the ground measurements) and the same boundary conditions are used for both simulations, the background errors at the upper levels are very small. By contrast, the numerical noise can become significant and leads to short length correlations at high levels. A similar behaviour is shown in Benedetti and Fisher (2007); Pagowski et al. (2010). In the DA experiments, we should therefore use a horizontal

Table 2. DA tests with different configurations for Balgovind Scale Parameters. AB stands for AirBase. Col. stands for column. × indicates the type of DA runs used (AirBase DA or Column DA).

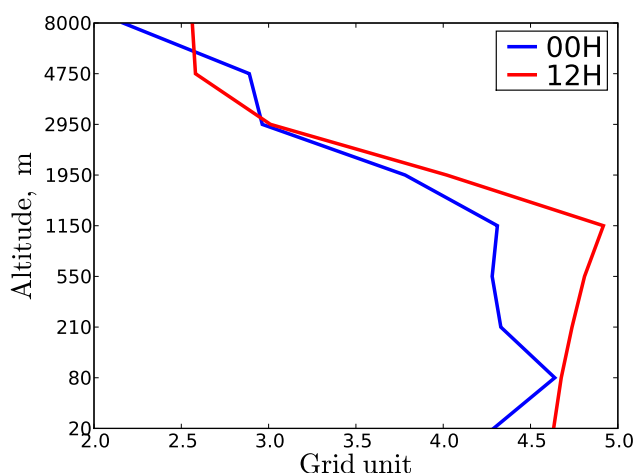| Simulation name	AirBase DA	Column DA	L_h (km)	L_v (m)
AB 50 km 1500 m	×		50	1500
AB 200 km 250 m	×		200	250
AB 200 km 1500 m	×		200	1500
AB 200 km 50/1500 m	×		200	50 (nighttime)
				1500 (daytime)
AB 400 km 1500 m	×		400	1500
Col. 50 km 0 m		×	50	0
Col. 200 km 0 m		×	200	0
Col. 400 km 0 m		×	400	0

Fig. 7. The blue (resp. red) line shows the horizontal correlation length L_h (grid unit) at 00:00 UTC (resp. 12:00 UTC) versus altitude. Note that a grid unit is about 50 km.

correlation length scale of 200 km. The Lidar In-Space Technology Experiment (LITE) (Winker et al., 1996) data suggest that aerosol fields have a horizontal correlation length scale of 200 km. Similarly to the horizontal correlation length, we find that the vertical correlation length L_v is about 250 m at the ground level.

Although the NMC method gives us estimates of the horizontal and vertical correlation lengths, DA tests with different correlation lengths are performed to assess the optimum lengths, i.e., the lengths which lead to the best forecast. The different tests performed are summarised in Table 2. Assimilation is performed with three different horizontal lengths: $L_h = 50$ km, $L_h = 200$ km and $L_h = 400$ km. For AirBase DA, assimilation is also performed with three different vertical correlation lengths: $L_v = 250$ m, $L_v = 1500$ m and L_v varying between nighttime and daytime. Because lidar provides us vertical profiles, the lidar DA can directly correct PM$_{10}$ concentrations at each model level (higher than 200 m above the ground). Therefore, we do not consider

L_v in the background error covariance matrix (we assume $L_v = 0$). Moreover, column DA tests with different L_v show that $L_v \neq 0$ does not lead to a better forecast for the column DA run. The scores (RMSE and correlation) calculated over land grid points from the ground level to the sixth level (1950 m above the ground) are shown in Fig. 8. Because only the initial conditions (pollutant concentrations) are different between the nature run and the control runs (see Sect. 4.3), and because the influence of initial conditions fades out with the forecast time, all control runs converge (RMSEs decrease to 0 and correlations increase to 1 in Fig. 8). The role of DA is to accelerate this convergence, to make RMSEs decrease and correlations increase faster. For AirBase DA, choosing $L_v = 1500$ m (DA test "AB 200km 1500m") leads to better scores (lower RMSE and lower correlation) than choosing $L_v = 250$ m (DA test "AB 200km 250m"), as estimated from the NMC method. Choosing $L_v = 50$ m in the nighttime and $L_v = 1500$ m in the daytime (DA test "AB 200km 50/1500m") does not lead to better scores than $L_v = 1500$ m (DA test "AB 200km 1500m"). A possible explanation is that the particles are mixed by turbulence more effectively in the model than in the true state of the atmosphere. The comparison of DA tests "AB 50km 1500m", "AB 200km 1500m" and "AB 400km 1500m" for AirBase and DA tests "Col. 50km 0m", "Col. 200km 0m" and "Col. 400km 0m" for the lidar network shows that $L_h = 200$ km, as estimated from the NMC method, leads to good scores. The scores are better than with $L_h = 50$ km, and similar to those obtained with $L_h = 400$ km.

We also studied the sensitivity of the results to the maximum altitude at which PM$_{10}$ DA is performed during the column DA. We tested the column DA until the eighth level (4750 m above the ground) instead of the sixth level (1950 m above the ground). We found small differences between the PM$_{10}$ forecasts at the ground level. It is mostly because the planetary boundary layer (PBL) is usually lower than 2000 m, and PM$_{10}$ concentrations above the PBL have limited impact on surface PM$_{10}$.
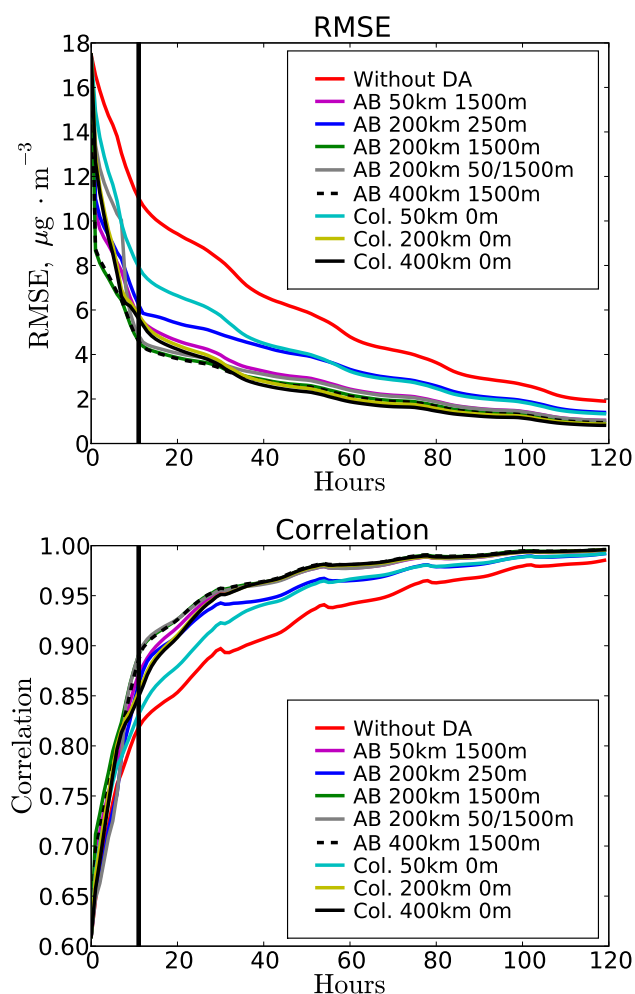
Fig. 9. RMSE (in $\mu g\,m^{-3}$) computed over land grid points from the ground to the sixth level (1950 m above the ground) for PM_{10} one-day forecast without DA (white columns), with the AirBase DA (grey columns) and with the column DA (blue columns).

Fig. 8. Top (resp. bottom) figure shows the time evolution of the RMSE in $\mu g\,m^{-3}$ (resp. correlation) of PM_{10} averaged over the different DA tests from 15 July to 10 August 2001. The scores are computed over land grid points from the ground to the sixth level (1950 m above the ground). The forecast is performed either without DA (red lines), or after AirBase DA or after column DA. The vertical black lines denote the separation between the assimilation period (to the left of the black lines) and the forecast (to the right of the black lines).

6 Comparison between AirBase and 12 lidars network DA

In the following, we compare the DA test "AB 200km 1500m" of Fig. 8 for AirBase ($L_h = 200$ km and $L_v = 1500$ m) and the DA test "Col. 200km 0m" of Fig. 8 for the lidar network ($L_h = 200$ km and $L_v = 0$).

Overall, the simulations with DA lead to better scores (lower RMSE and higher correlations) than the simulation without DA. But as shown in Tombette et al. (2009), the assimilation procedure has almost no impact on PM_{10} concentrations after several days of forecast, because assimilation influences only initial conditions of the forecast period and
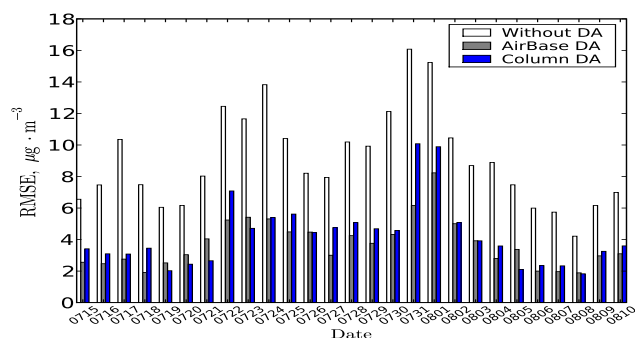
the influence of initial conditions on PM_{10} concentrations does not last for more than a few days. The AirBase DA forecast has always better scores than the column DA forecast in the first several hours of assimilation (to the left of the black line). This may be explained by the fact that the AirBase DA run assimilates from the first level of the model (20 m above the ground) to the sixth level (1950 m above the ground) and the column DA run assimilates from the third level (210 m above the ground) to the sixth level (1950 m above the ground). It takes several hours for the column DA to influence ground concentrations.

However, during the forecast period, the RMSE of the column DA run decreases faster than the AirBase DA run (to the right of the black line). After 24 hours forecast, the column DA has better scores than the AirBase DA run. It is mostly because the impact of the column DA run is higher than the AirBase DA run at high levels.

Figure 9 shows the RMSE for the PM_{10} forecast without DA, with the AirBase DA and with the column DA for each one-day forecast period between 15 July and 10 August. Assimilation improves the forecast RMSE for each forecast. The averaged RMSE over all forecasts is $9.1\,\mu g\,m^{-3}$ without DA, $3.7\,\mu g\,m^{-3}$ (59 % less) with the AirBase DA and $4.2\,\mu g\,m^{-3}$ (54 % less) with the column DA. Although the AirBase DA leads to lower RMSE than the column DA for most forecasts in Fig. 9, the column DA can also lead to lower or similar RMSE as the AirBase DA for some forecasts, e.g. the forecasts starting 19, 20, 21, 23, 26 July and 3, 5, 8 August. It is mostly because the lidar network provides more accurate information than AirBase on those days at high altitude, e.g. Sahara dust in Madrid as shown in Fig. 3 (upper panel).

Figure 10 shows the RMSE for the PM_{10} forecast without DA, with the AirBase DA and with the column DA during the second forecast day for each experiment between 15 July and 10 August. The averaged RMSE over all forecasts is $6.1\,\mu g\,m^{-3}$ without DA, $2.7\,\mu g\,m^{-3}$ (56 % less) with the AirBase DA and $2.6\,\mu g\,m^{-3}$ (57 % less) with the column DA.
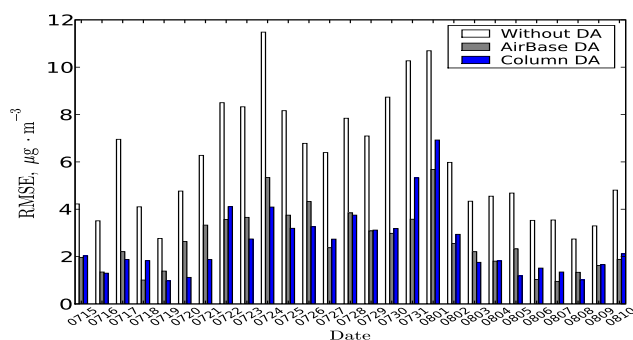
Fig. 10. RMSE (in $\mu g\,m^{-3}$) computed over land grid points from the ground to the sixth level (1950 m above the ground) for PM_{10} second forecast day without DA (white columns), with the AirBase DA (grey columns) and with the column DA (blue columns).

For the second forecast day (Fig. 10), the relative impact of column DA and AirBase DA is different from the first forecast day (Fig. 10) : the column DA leads to lower or similar RMSE as the AirBase DA for most forecasts.

The results show that the impact on PM_{10} forecast of assimilating data from a lidar network with 12 stations and data from a ground network AirBase with 488 stations are similar in terms of scores, although AirBase (resp. lidar) DA leads to slightly better scores for the first (resp. second) forecast day. We will study the sensitivity to the number and to the lidar locations in the next section.

7 Sensitivity to the number and position of lidars

In this section, we study the sensitivity of the results to the number and to the locations of lidars. Forecasts after DA with four different lidar networks are compared to DA with the previously-used lidar network (blue discs in Fig. 11). Data assimilation is performed with another lidar network of 12 lidar stations (denoted Network 12, yellow discs in Fig. 11), with a lidar network of 26 stations (denoted Network 26, magenta diamonds in Fig. 11), with a lidar network of 76 stations (denoted Network 76, cyan thin diamonds in Fig. 11) and DA with a lidar network made of all AirBase stations over western Europe (denoted Network 488, the red triangles in Fig. 1).

Figures 12 and 13 show the time evolution of the RMSE and the correlation respectively, averaged over all land grids and the vertical for the different tests. Comparing the previously-used lidar network with Network 12 in Fig. 11, we can see that although they have the same number of stations, the locations are very different. Because the stations of Network 12 are more regularly spaced than the stations of the previously-used lidar network, Network 12 stations are better spread out over Europe than the previously-used lidar network. Network 12 leads to better scores in the first forecast day than the reference network. This shows that the li-
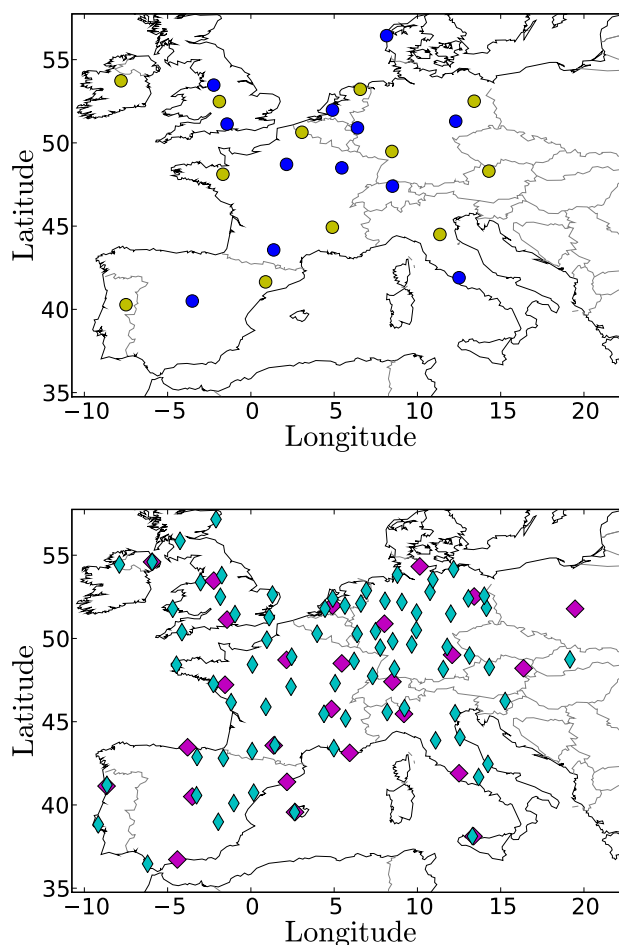

Fig. 11. Four potential lidar networks in Europe. The blue discs in the top figure show the locations of the reference lidar network. The yellow discs in the top figure show the locations of the lidar Network 12. The magenta diamonds in the bottom figure show the locations of the lidar Network 26. The cyan thin diamonds in the bottom figure show the locations of the lidar Network 76.

dar stations need to be regularly distributed over Europe for an overall improvement of the PM_{10} forecast. The lidar networks 26, 76 and 488 which have more lidar stations perform better (lower RMSE, higher correlation) than the two others. The lidar network 26 DA run has less than $0.15\,\mu g\,m^{-3}$ of RMSE higher than AirBase DA at the beginning of forecast window and has a better score than AirBase DA run after several hours forecast. If one increases the number of lidar stations from 26 to 76, the lidar network 76 DA run has better scores than the AirBase DA run at the beginning of the forecast window and has better scores than the AirBase DA during the forecast days. If one increases the number of lidar stations to 488 (the same as the number of AirBase stations), the lidar network 488 DA run has much better scores than the AirBase DA run during the forecast days. Although increasing the number of lidar gives better forecast scores, such lidar networks may be too expensive.
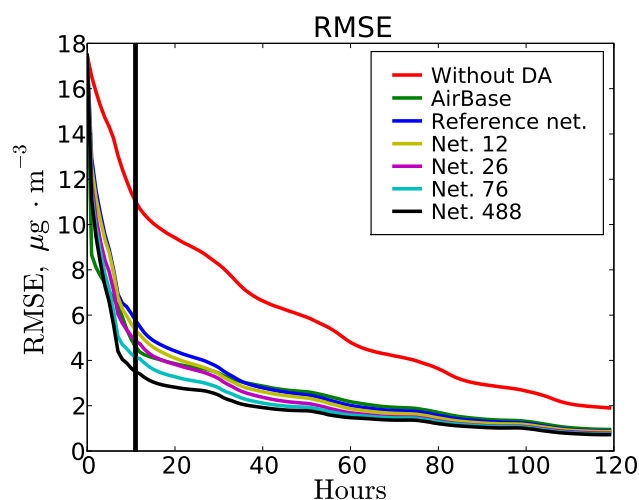
Fig. 12. Hourly evolution of the RMSE (in µg m^{-3}) of PM$_{10}$ averaged over the different experiments from 15 July to 10 August 2001. The RMSE is computed over land grid points from the ground to the sixth level (1950 m above the ground). The runs are performed without DA (red line), with AirBase DA (green line), with the reference lidar network DA (12 stations, blue line), with Network 12 DA (12 stations, yellow line), with Network 26 DA (26 stations, magenta line), with Network 76 DA (76 stations, cyan line) and with Network 488 DA (488 stations, black line). Net. stands for network.
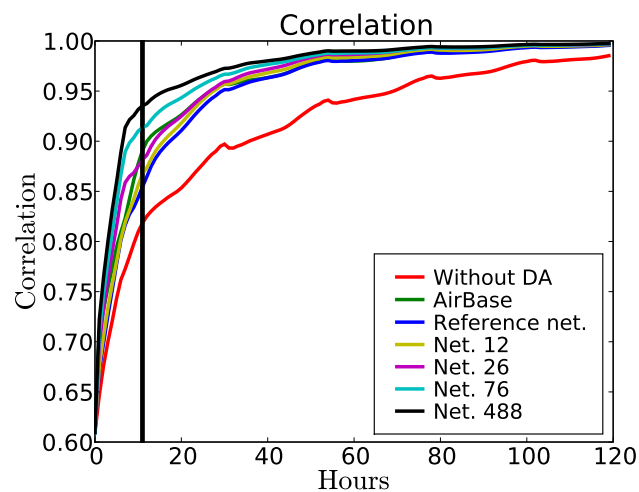

Fig. 13. Hourly evolution of the PM$_{10}$ correlation averaged over the different experiments from 15 July to 10 August 2001. The correlation is computed over land grid points from the ground to the sixth level (1950 m above the ground). The runs are performed without DA (red line), with AirBase DA (green line), with the reference lidar network DA (12 stations, blue line), with Network 12 DA (12 stations, yellow line), with Network 26 DA (26 stations, magenta line), with Network 76 DA (76 stations, cyan line) and with Network 488 DA (488 stations, black line).

8 Conclusions

In order to investigate the potential impact of a ground-based lidar network on short-term forecasts of PM$_{10}$, an OSSE has been implemented. Because the AirBase network covers well western Europe and provides in situ surface measurements and because AirBase measurements have been used for DA of PM$_{10}$, we took AirBase as an assimilation reference network. We have compared the impacts of assimilating ground-based lidar network data to assimilating the AirBase surface network data.

Because we made several simplifying assumptions: we used an identical twin scenario (perfect model) and assumed uncorrelated observational errors, the PM$_{10}$ improvements from assimilating lidar and ground observations may be over optimistic. Compared to the RMSE for one-day forecasts without DA, the RMSE between one-day forecasts and the truth states is improved on average over the summer month from 15 July to 15 August 2001 by 54 % by the lidar DA with 12 lidars, and by 59 % by the AirBase DA. For the second forecast days, compared to the RMSE for second forecast days without DA, the RMSE is improved on average over the summer month from 15 July to 15 August 2001 by 57 % by the lidar DA, and by 56 % by the AirBase DA. Although AirBase DA can correct PM$_{10}$ concentrations at high levels because of the long vertical correlation length of the background errors, the lidar DA corrects PM$_{10}$ concentrations more accurately than the AirBase DA at high levels. The spatial and temporal influence of the assimilation of lidar observations is larger and longer. The results shown in this paper suggest that the assimilation of lidar observations would improve PM$_{10}$ forecast over Europe.

As lidar stations are developing over Europe following volcanic eruptions in Iceland (Chazette et al., 2012; Pappalardo et al., 2010), a sensitivity analysis has also been conducted on the number and locations of lidars. We found that spreading out the lidars regularly over Europe can improve the PM$_{10}$ forecast. Compared to the RMSE for one-day forecasts without DA, the RMSE between one-day forecast and the truth states is improved on average over the summer month from 15 July to 15 August 2001 by 57 % by the lidar DA with 12 optimised lidars, and by 59 % by the AirBase DA. Increasing the number of lidar improves the forecast scores. For example, the improvement of the RMSE becomes as high as 65 % (compared to the RMSE for one-day forecasts without DA) if 76 lidars are used, but a lidar network with many stations may be too expensive.

For future works, we will use real measurements from lidar stations, directly assimilating the lidar signals in the chemistry transport model and performing DA with a combination of lidar and AirBase observations.

Appendix A

Statistical indicators

Let $\{o_i\}_{i=1,n}$ and $\{s_i\}_{i=1,n}$ be the observed and the modelled concentrations, respectively. Let n be the number of available observations. The statistical indicators used to evaluate the results with respect to the truth are: the Root Mean Square Error (RMSE), the (Pearson) correlation, the Mean Fractional Error (MFE), the Mean Fractional Bias (MFB). MFE and MFB bound the maximum error and bias and do not allow a few data points to dominate the statistics. They are often used to evaluate model performances against observations for aerosols (Boylan and Russel, 2006). The RMSE is a measure of the extent that the model deviates from the observations. Correlation is a measure of statistical relationships involving dependence between the observed and the modelled concentrations. The statistical indicators are defined as follow:

$$\text{RMSE} = \sqrt{\frac{1}{n}\sum_{i=1}^{n}(o_i - s_i)^2}, \tag{A1}$$

$$\text{correlation} = \frac{\sum_{i=1}^{n}(o_i - \bar{o})(s_i - \bar{s})}{\sqrt{\sum_{i=1}^{n}(o_i - \bar{o})^2 \sum_{i=1}^{n}(s_i - \bar{s})^2}}, \tag{A2}$$

$$\text{MFE} = \frac{1}{n}\sum_{i=1}^{n}\frac{|s_i - o_i|}{(s_i + o_i)/2}, \tag{A3}$$

$$\text{MFB} = \frac{1}{n}\sum_{i=1}^{n}\frac{s_i - o_i}{(s_i + o_i)/2}, \tag{A4}$$

where $\bar{o} = \frac{1}{n}\sum_{i=1}^{n}o_i$ and $\bar{s} = \frac{1}{n}\sum_{i=1}^{n}s_i$.

References

Baker, D. F., BÖsch, H., Doney, S. C., O'Brien, D., and Schimel, D. S.: Carbon source/sink information provided by column CO_2 measurements from the Orbiting Carbon Observatory, Atmos. Chem. Phys., 10, 4145–4165, doi:10.5194/acp-10-4145-2010, 2010.

Balgovind, R., Dalcher, A., Ghil, M., and Kalnay, E.: A Stochastic-Dynamic Model for the Spatial Structure of Forecast Error Statistics, Mon. Weather Rev., 111, 701–722, 1983.

Barker, J. and Tingey, D. T. : Air Pollution Effects on Biodiversity, 304 pp., Springer, New York, USA, 1992.

Benedetti, A. and Fisher, M. : Background error statistics for aerosols, Q. J. Roy. Meteor. Soc., 133, 391–405, 2007.

Berthier, S., Chazette, P., Couvert, P., Pelon, J., Dulac, F., Thieuleux, F., Moulin, C., and Pain T. : Desert dust aerosol columnar properties over ocean and continental Africa from Lidar in-Space Technology Experiment (LITE) and Meteosat synergy, J. Geophys. Res., 111, D21202, doi:10.1029/2005JD006999, 2006.

Bouttier, F. and Courtier, P.: Data assimilation concepts and methods, Meteorological Training Course Lecture Series, ECMWF, 2001.

Boylan, J. W. and Russell, A. G.: PM and light extinction model performance metrics, goals, and criteria for three-dimensional air quality models, Atmos. Environ., 40, 4946–4959, 2006.

Brandt, J., Christensen, J. H., Frohn, L. M., Geels, C., Hansen, K. M., Hedegaard, G. B., Hvidberg, M. and Skjøth, C. A.: THOR – an operational and integrated model system for air pollution forecasting and management from regional to local scale. Proceedings of the 2nd ACCENT Symposium, Urbino (Italy), 23–27 July, 2007.

Chazette, P., Randriamiarisoa, H., Sanak, J., and Couvert P.: Optical properties of urban aerosol from airborne and ground-based in situ measurements performed during the ESQUIF program, J. Geophys. Res, 110, D02206, doi:10.1029/2004JD004810, 2005.

Chazette, P., Sanak, J., and Dulac, F. : New Approach for Aerosol Profiling with a Lidar Onboard an Ultralight Aircraft: Application to the African Monsoon Multidisciplinary Analysis, Environ. Sci. Technol., 41, 8335–8341, 2007.

Chazette, P., Raut, J.-C., Dulac, F., Berthier, S., Kim, S.-W., Royer, P., Sanak, J., Loaëc, S., and Grigaut-Desbrosses, H.: Simultaneous observations of lower tropospheric continental aerosols with a ground-based, an airborne, and the space-borne CALIOP lidar systems, J. Geophys. Res., 115, D00H31, doi:/10.1029/2009JD012341, 2010.

Chazette, P., Bocquet, M., Royer, P., Winiarek, V., Raut, J.-C., Labazuy, P., Gouhier, M., Lardier, M., and Cariou J.-P.: Eyjafjallajökull ash concentrations derived from both Lidar and modeling, J. Geophys. Res. Atmos., 117, D00U14, doi:10.1029/2011JD015755, 2012.

Chen, S.-H., Chen, J.-Y., Chang, W.-Y., Lin, P.-L., Lin, P.-H., and Sun, W.-Y.: Observing System Simulation Experiment: Development of the system and preliminary results, J. Geophys. Res., 116, D13202, doi:10.1029/2010JD015103, 2011.

Chevallier, F., Bréon, F.-M., and Rayner, P. J.: Contribution of the Orbiting Carbon Observatory to the estimation of CO2 sources and sinks: Theoretical study in a variational data assimilation framework, J. Geophys. Res., 112, D09307, 11 pp., doi:10.1029/2006JD007375, 2007.

Chin, M., Rood, R. B., Lin, S.-J., Müller, J.-F., and Thompson, A. M.: Atmospheric sulfur cycle simulated in the global model GOCART: Model description and global properties, J. Geophys. Res., 105, 24671–24687, 2000.

Claeyman, M., Attié, J.-L., Peuch, V.-H., El Amraoui, L., Lahoz, W. A., Josse, B., Joly, M., Barré, J., Ricaud, P., Massart, S., Piacentini, A., von Clarmann, T., HÖpfner, M., Orphal, J., Flaud, J.-M., and Edwards, D. P.: A thermal infrared instrument onboard a geostationary platform for CO and O_3 measurements in the lowermost troposphere: Observing System Simulation Experiments (OSSE), Atmos. Meas. Tech., 4, 1637–1661, doi:10.5194/amt-4-1637-2011, 2011.

Daley, R.: Atmospheric data analysis, Cambridge University Press, 1991.

De Wildt, MD., Eskes, H., Manders, A., Sauter, F., Schaap, M., Swart, D., and van Velthoven, P.: Six-day PM_{10} air quality forecasts for the Netherlands with the chemistry transport model Lotos-Euros, Atmos. Environ., 45, 5586–5594, doi:10.1016/j.atmosenv.2011.04.049, 2011.

Debry, E., Fahey, K., Sartelet, K., Sportisse, B., and Tombette, M.: Technical Note: A new SIze REsolved Aerosol Model (SIREAM), Atmos. Chem. Phys., 7, 1537–1547, doi:10.5194/acp-7-1537-2007, 2007.

Denby, B., Schaap, M., Segers, A., Builtjes, P., and Horálek, J.: Comparison of two data assimilation methods for assessing PM_{10} exceedances on the European scale, Atmos. Environ., 42, 7122–7134, 2008.

Dickerson, R. R., Kondragunta, S., Stenchikov, G., Civerolo, K. L., Doddrige, B. G., and Holben, B. N.: The impact of aerosols on solar ultraviolet radiation and photochemical smog, Science, 278, 827–830, 1997.

Dockery, D. and Pope, A.: Epidemiology of acute health effects: summary of time-series, in: Particles in Our Air: Concentration and Health Effects, edited by: Wilson, R. and Spengler, J. D., Harvard University Press, Cambridge, MA, USA, 123–147, 1996.

Edwards, D. P., Arellano Jr., A. F., and Deeter, M. N.: A satellite observation system simulation experiment for carbon monoxide in the lowermost troposphere, J. Geophys. Res., 114, D14304, doi:10.1029/2008JD011375, 2009.

Elbern, H., Schwinger, J., and Botchorishvili, R.: Chemical state estimation for the middle atmosphere by four-dimensional variational data assimilation: System configuration, J. Geophys. Res.-Atmos., 115, D06302, doi:10.1029/2009JD011953, 2010.

Hodzic, A., Vautard, R., Chazette, P., Menut, L., and Bessagnet, B.: Aerosol chemical and optical properties over the Paris area within ESQUIF project, Atmos. Chem. Phys., 6, 3257–3280, doi:10.5194/acp-6-3257-2006, 2006.

Horowitz, L., Walters, S., Mauzerall, D., Emmons, L., Rasch, P., Granier, C., Tie, X., Lamarque, J.-F., Schultz, M., Tyndall, G., Orlando, J., and Brasseur, G.: A global simulation of tropospheric ozone and related tracers: Description and evaluation of MOZART, version 2, J. Geophys. Res., 108, 4784, 25 pp., doi:10.1029/2002JD002853, 2003.

Intergovernment Panel on Climate Control(IPCC): Climate Change 2007, the fourth Assessment Report of the IPCC, Cambridge Univ. Press, New York, USA, 2007.

Kalnay, E.: Atmospheric modeling, data assimilation, and predictability, Cambridge University Press, 341 pp., 2003.

Kaufman, Y. J., Tanré, D., and Boucher, O.: A satellite view of aerosols in the climate system. Nature, 419, 215–223, 2002.

Kim, Y., Sartelet, K. N., and Seigneur, C.: Comparison of two gas-phase chemical kinetic mechanisms of ozone formation over Europe, J. Atmos. Chem., 62, 89–119, 2010.

Kim, Y., Sartelet, K., and Seigneur, C.: Formation of secondary aerosols over Europe: comparison of two gas-phase chemical mechanisms, Atmos. Chem. Phys., 11, 583–598, doi:10.5194/acp-11-583-2011, 2011.

Kim, Y., Couvidat, F., Sartelet, K., and Seigneur, C.: Comparison of different gas-phase mechanisms and aerosol modules for simulating particulate matter formation. J. Air Waste Manage. Assoc., 61, 1218–1226, doi:10.1080/104732.89.2011.603939, 2011.

Klett, J. D.: Stable analytical inversion solution for processing lidar returns, Appl. Optics, 20, 211-220, 1981.

Konovalov, I. B., Beekmann, M., Meleux, F., Dutot, A., and Foret, G.: Combining deterministic and statistical approaches for $PM_{(10)}$ forecasting in Europe, Atmos. Environ., 43, 6425–6434, doi:10.1016/j.atmosenv.2009.06.039, 2009.

Kuo, Y.-H. and Anthes, R. A.: Accuracy of diagnostic heat and moisture budgets using SESAME-79 field data as revealed by observing system simulation experiments, Mon. Weather Rev., 112, 1465–1481, 1984.

Lahoz, W., Khattatov, B., and Ménard, R. (Eds.): Data Assimilation Making Sense of Observations, Springer, Berlin, Germany, 718 pp., 2010.

Lauwerys, R., Haufroid, V., Hoet, P., and Lison, D.: Toxicologie industrielle et intoxications professionnelles, Masson, 1252 pp., 2007.

Léon, J. F., Chazette, P., Pelon, J., Dulac, F., and Ramdriamarisoa, H.: Aerosol direct radiative impact over the INDOEX area based on passive and active remote sensing, J. Geophys. Res., 107, 8006, doi:10.1029/2000JD000116, 2002.

Liu, J. and Kalnay, E.: Simple Doppler wind lidar adaptive observation experiments with 3D-Var and an ensemble Kalman filter in a global primitive equations model, Geophys. Res. Lett., 34, L19808, doi:10.1029/2007GL030707, 2007.

Mallet, V., Quélo, D., Sportisse, B., Ahmed de Biasi, M., Debry, É., Korsakissok, I., Wu, L., Roustan, Y., Sartelet, K., Tombette, M., and Foudhil, H.: Technical Note: The air quality modeling system Polyphemus, Atmos. Chem. Phys., 7, 5479–5487, doi:10.5194/acp-7-5479-2007, 2007.

Masutani, M., Woolen, J. S., Lord, S. J., Emmitt, G. D., Kleespies, T. J., Wood, S. A., Greco, S., Sun, H, Terry, J., Kapoor, V., Treadon, R., and Campana, K. A.: Observing system simulation experiments at the National Centers for Environmental Prediction, J. Geophys. Res., 115, D07101, doi:10.1029/2009JD012528, 2010.

Niu, T., Gong, S. L., Zhu, G. F., Liu, H. L., Hu, X. Q., Zhou, C. H., and Wang, Y. Q.: Data assimilation of dust aerosol observations for the CUACE/dust forecasting system, Atmos. Chem. Phys., 8, 3473–3482, doi:10.5194/acp-8-3473-2008, 2008.

Pagowski, M., Grell, G. A., McKeen, S. A., Peckham, S. E., and Devenyi, D.: Three-dimensional variational data assimilation of ozone and fine particulate matter observations: some results using the Weather Research and Forecasting – Chemistry model and Grid-point Statistical Interpolation, Q. J. Roy. Meteorol. Soc., 136, 2013–2024, doi:10.1002/qj.700, 2010.

Pappalardo, G, Amodeo, A., Ansmann, A., Apituley, A., Arboledas, L.A., Balis, D., Böckmann, C., Chaikovsky, A., Comeron, A., D'Amico, G., De Tomasi, F., Freudenthaler, V., Giannakaki, E., Giunta, A., Grigorov, I., Gustafsson, O., Gross, S., Haeffelin, M., Iarlori, M., Kinne, S., Linné, H., Madonna, F., Mamouri, R., Mattis, I., McAuliffe, M., Molero, F., Mona, L., Müller, D., Mitev, V., Nicolae, D., Papayannis, A., Perrone, M.R., Pietruczuk, A., Pujadas, M., Putaud, J. P., Ravetta, F., Rizi, V., Serikov, I., Sicard, M., Simeonov, V., Spinelli, N., Stebel, K., Trickl, T., Wandinger, U., Wang, X., Wagner, F., and Wiegner, M. : EARLINET observations of the Eyjafjallajökull ash plume over Europe, SPIE Proceedings, 7832, doi:10.1117/12.869016, 2010.

Parrish, D. F. and Derber, J. C.: The National Meteorological Center's spectral statistical interpolation analysis system, Mon. Weather Rev., 120, 1747–1763, 1992.

Perez, C., Sicard, M., Jorba, O., Comeron, A., and Baldasano, J. M.: Summertime re-circulations of air pollutants over the northeastern Iberian coast observed from systematic EARLINET lidar measurements in Barcelona, Atmos. Environ., 38, 3983–4000, 2004.

Randriamiarisoa, H., Chazette, P., and Mégie, G.: The columnar retrieved single scattering albedo from NO_2 photolysis rate, Tellus, Ser. B, 56, 118–127, 2004.

Randriamiarisoa, H., Chazette, P., Couvert, P., Sanak, J., and Mégie, G. : Relative humidity impact on aerosol parameters in a Paris suburban area, Atmos. Chem. Phys., 6, 1389–1407, doi:10.5194/acp-6-1389-2006, 2006.

Ramanathan, V., Crutzen, P. J., Lelievald, J., Mitra, A. P., Althausen, D., Anderson, J., Andreae, M. O., Cantrell, W., Cass, G. R., Chung, C. E., Clarke, A. D., Coakley, J. A., Collins, W. D., Conant, W. C., Dulac, F., Heintzenberg, J., Heymsfield, A. J., Holben, B., Howell, S., Hudson, J., Jayaraman, A., Kiehl, J. T., Krishnamurti, T. N., Lubin, D., McFarquhar, G., Novakov, T., Ogren, J. A., Podgorny, I. A., Prather, K., Priestley, K., Prospero, J. M., Quinn, P. K., Rajeev, K., Rasch, P., Rupert, S., Sadourny, R., Satheesh, S. K., Shaw, G. E., Sheridan, P., and Valero, F. P. J.: Indian Ocean Experiment: An integrated analysis of the climate forcing and effects of the great Indo-Asian haze, J. Geophys. Res., 106, 28371–28398, 2001.

Roustan, Y., Sartelet, K. N., Tombette, M., Debry, É., and Sportisse, B.: Simulation of aerosols and gas-phase species over Europe with the POLYPHEMUS system. Part II: Model sensitivity analysis for 2001, Atmos. Environ., 44, 4219–4229, 2010.

Raut, J.-C. and Chazette, P.: Retrieval of aerosol complex refractive index from a synergy between lidar, sunphotometer and in situ measurements during LISAIR experiment, Atmos. Chem. Phys., 7, 2797–2815, doi:10.5194/acp-7-2797-2007, 2007.

Raut, J.-C. and Chazette, P.: Assessment of vertically-resolved PM_{10} from mobile lidar observations, Atmos. Chem. Phys., 9, 8617–8638, doi:10.5194/acp-9-8617-2009, 2009.

Royer, P., Chazette, P., Sartelet, K., Zhang, Q. J., Beekmann, M., and Raut, J.-C.: Comparison of lidar-derived PM_{10} with regional modeling and ground-based observations in the frame of MEGAPOLI experiment, Atmos. Chem. Phys., 11, 10705–10726, doi:10.5194/acp-11-10705-2011, 2011.

Sartelet, K. N., Debry, E., Fahey, K. M., Roustan, Y., Tombette, M., and Sportisse, B. : Simulation of aerosols and gas-phase species over Europe with the Polyphemus system. Part I: model-to-data comparison for 2001, Atmos. Environ., 29, 6116–6131, 2007.

Schaap, M., Spindler, G., Schulz, M., Acker, K., Maenhaut, W., Berner, A., Wieprecht, W., Streit, N., Müller, K., Brüggemann, E., Chi, X., Putaud, J.-P., Hitzenberger, R., Puxbaum, H, Baltensperger, U., and ten Brink, H.: Artefacts in the sampling of nitrate studied in the "INTERCOMP" campaigns of EUROTRAC-AEROSOL, Atmos. Environ., 48, 6487–6496, 2004.

Sheridan, P. J., Jefferson, A., and Ogren, J. A.: Spatial variability of submicrometer aerosol radiative properties over the Indian Ocean during INDOEX, J. Geophys. Res., 107, 8011, doi:10.1029/2000JD000166, 2002.

Simpson, D., Fagerli, H., Jonson, J. E., Tsyro, S., Wind, P., and Tuovinen, J.-P.: Transboundary acidification, euthrophication and ground level ozone in Europe. Part I: unified EMEP model description, Technical Report, EMEP, 2003.

Tan, D. G. H., Andersson, E., Fisher, M., and Isaksen, L.: Observing system impact assessment using a data assimilation ensemble technique: application to the ADM-Aeolus wind profiling mission, Q. J. Roy. Meteorol. Soc., 133, 381–390, 2007.

Timmermans, R. M. A., Segers, A. J., Builtjes, P. J. H., Vautard, R., Siddans, R., Elbern, H., Tjemkes, S. A. T., and Schaap, M.: The added value of a proposed satellite imager for ground level particulate matter analyses and forecasts, IEEE J. Sel. Topics Appl. Earth Obs. Remote Sens., 2, 271–283, 2009.

Tombette, M., Mallet, V., and Sportisse, B.: PM_{10} data assimilation over Europe with the optimal interpolation method, Atmos. Chem. Phys., 9, 57–70, doi:10.5194/acp-9-57-2009, 2009.

Winker, D. M., Couch, R. H., and McCormick, M. P.: An overview of LITE: NASA's Lidar In-space Technology Experiment, Proc. IEEE, 84, 164–180, 1996.

Winker, D. M., Pelon, J., and McCormick, M. P.: The CALIPSO mission: Spaceborne lidar for observation of aerosols and clouds, Proc. SPIE, 4893, doi:10.1117/12.466539, 2003.

Wu, L., Mallet, V., Bocquet, M., and Sportisse, B.: A comparison study of data assimilation algorithms for ozone forecasts, J. Geophys. Res., 113, D20310, doi:10.1029/2008JD009991, 2008.

Yarwood, G., Rao, S., Yocke, M., and Whitten, G.: Updates to the Carbon Bond Chemical Mechanism: CB05 Final Report to the US EPA, RT-0400675, available at: http://www.camx.com/publ/pdfs/CB05_Final_Report_120805.pdf, 2005.

Zhang, Y., Bocquet, M., Mallet, V., Seigneur, C., and Baklanov, A.: Real-time air quality forecasting, part II: State of the science, current research needs, and future prospects, Atmos. Environ., 60, 656–676, 2012.